

# Bloch band structures and linear response theory of nonlinear systems

Fude Li<sup>1</sup>, Junjie Wang<sup>1</sup>, Dianzhen Cui<sup>1</sup>, K. Xue<sup>1</sup>, and X. X. Yi<sup>1\*</sup>

<sup>1</sup>*Center for Quantum Sciences and School of Physics,  
Northeast Normal University, Changchun 130024, China*

(Dated: October 26, 2022)

We investigate the Bloch bands and develop a linear response theory for nonlinear systems, where the interplay between topological parameters and nonlinearity leads to new band structures. The nonlinear system under consideration is described by the Qi-Wu-Zhang model with Kerr-type nonlinearity, which can be treated as a nonlinear version of Chern insulator. We explore the eigenenergies of the Hamiltonian and discuss its Bloch band structures as well as the condition of gap closing. A cone structure in the ground Bloch band and tubed structure in the excited Bloch band is found. We also numerically calculate the linear response of the nonlinear Chern insulator to external fields, finding that these new band structures break the condition of adiabatic evolution and make the linear response not quantized. This feature of response can be understood by examining the dynamics of the nonlinear system.

## I. INTRODUCTION

In the last decades, the rapid development of topological band theory in condensed matter physics[1–5] has found applications in many materials, such as topological insulators[6–12], topological semimetals[13–16], and topological crystalline insulators[17–21]. Topology of energy bands structures of these materials offer us a new method to classify different quantum phases with topological invariant[1, 22–25] and lead to many fascinating phenomena including topological pumps and quantized conductance. The linear response of topological materials to external fields can be described by topological invariants. For example, quantized Hall conductance is proportional to Chern numbers, which can be verified by the linear response of these electronic systems to external electronic fields.

Recently, topological concepts developed for electric systems have been extended to study a variety of photonic fields[26–31] such as photonic crystals[32–34], waveguide arrays[35–39] and ring resonators[40–42]. These systems possess topological band structure similar to the electric systems. In this sense, topological band structures can be realized (or simulated) and observed in photonic systems[43–45]. Due to the manufacturing flexibility, optical systems may offer more modulating parameters than their electric counterparts including non-linear couplings.

Combining these topological photonic structures with nonlinear effects, we will make a step forward in the emerging field of nonlinear topological photonics, which would fill the gap between the physics of topological phases and nonlinear optics[46–60]. In fact, there are many publications in this field for two- or many-level systems. For example, looped structures are produced in one-dimensional systems[61–71], which have recently been realized experimentally[72–75]. For Bloch band in

nonlinear systems, interplay between nonlinearity and band topology can lead to many interesting structures. Nonlinearities arising from photonic structures have an effect on topological phases[76–79] and trigger the appearance of new band structures[80–85], such as nonlinear Dirac cones and nonlinear Dirac points in two-dimensional systems. Generally, linear topological bands can be combined with mean-field interactions, which reduces any many-body problem into an one-body nonlinear problem. In the mean-field approximation, the discussions on the nonlinear systems are based on nonlinear Schrödinger equation with state-dependent Hamiltonian(nonlinear Hamiltonian), which is widely used to study emerging nonlinear features.

Except the study of the effect of nonlinearity on Bloch bands, here we also focus on the linear response of nonlinear systems to external field which plays a prominent role in many fields of physics. Intersection between linear topological bands and nonlinearity can give rise to the radical change of linear response of mean-field nonlinear systems. In contrast to the linear response in linear systems, the linear response of nonlinear systems to external field is not quantized and can not be characterized by topological invariant.

The reminder of this manuscript is organized as follows. In Sec. II, we develop a method to explore the Bloch band structures in a general nonlinear two-band systems. In Sec. III, we illustrate the method developed in the last section with a nonlinear Chern insulator. Band gap closing of the system is also discussed. In Sec. IV, we numerically calculate the linear response of nonlinear Chern insulator to external field and discuss the differences of linear response in linear and nonlinear systems. We consider adiabatic evolution of the system governed by the nonlinear Bloch Hamiltonian and study effects brought by the dynamics beyond the adiabatic evolution. In Sec. V, we examine the dynamics of the system to study whether the adiabatic evolution has an effect on the linear response of the system. In Sec. VI, we summarize our results.

---

\*Electronic address: [yixx@nenu.edu.cn](mailto:yixx@nenu.edu.cn)

## II. BLOCH BAND STRUCTURE FOR NONLINEAR SYSTEMS

We begin by presenting a method to find the eigenvalues of general nonlinear systems. To be specific, we consider a two-band system whose dynamics being governed by the following nonlinear Schrödinger equation

$$i\partial_t\Psi(t) = \hat{H}(t)\Psi(t) \quad (1)$$

with

$$\hat{H}(t) = \mathbf{d} \cdot \hat{\sigma} + U[|\psi_1(t)|^2, 0; 0, |\psi_2(t)|^2], \quad (2)$$

where  $\hat{\sigma} = (\sigma_x, \sigma_y, \sigma_z)$  are Pauli matrices acting on the pseudospin space, and  $\mathbf{d} = (d_x, d_y, d_z)$ . This Hamiltonian can be obtained by considering the Bloch form of a two-dimensional Bose-Hubbard Hamiltonian by the mean-field approximation in the limit of the large number of particles. And  $\Psi = [\psi_1(t), \psi_2(t)]^T$  denotes the time-dependent mean-field wave function. We consider the time-independent form  $\psi_j = \phi_j e^{-i\epsilon t/\hbar}$ ,  $j = 1, 2$ , and define the nonlinear Hamiltonian as

$$\hat{H} = \begin{pmatrix} d_z + U|\phi_1|^2 & d_x - id_y \\ d_x + id_y & -d_z + U|\phi_2|^2 \end{pmatrix}. \quad (3)$$

The time-independent nonlinear eigenvalues and corresponding eigenstates can be found by solving

$$\hat{H} \begin{pmatrix} \phi_1 \\ \phi_2 \end{pmatrix} = \epsilon \begin{pmatrix} \phi_1 \\ \phi_2 \end{pmatrix}. \quad (4)$$

Here these eigenstates correspond to stationary solutions of time-dependent nonlinear Schrödinger equation. Due to nonlinearity, more eigenenergies might appear in the system. This is one of the key differences between linear and nonlinear systems. To solve this eigenvalue equation, we set a new variable  $\kappa$ ,  $\kappa = |\phi_1|^2 - |\phi_2|^2$ , and use the normalization condition,  $|\phi_1|^2 + |\phi_2|^2 = 1$ . After tedious but straightforward calculations, the relation between  $\kappa$  and  $\epsilon$  is given by

$$(\epsilon - U)\kappa = d_z, \quad (5)$$

and the eigenstates,  $|\phi_1|^2$  and  $|\phi_2|^2$ , are given by

$$\begin{aligned} |\phi_1|^2 &= \frac{1}{2} + \frac{d_z}{2(\epsilon - U)}, \\ |\phi_2|^2 &= \frac{1}{2} - \frac{d_z}{2(\epsilon - U)}, \end{aligned} \quad (6)$$

where we replace  $\kappa$  with  $\epsilon$ , and get an  $\epsilon$ -dependent nonlinear Hamiltonian useful for our calculations. In linear regime, the eigenvalues can be obtained from  $|H - \epsilon| = 0$ . In nonlinear regime, this condition is the same as in the linear regime. Setting the determinant be zero,

$$\begin{vmatrix} d_z + \frac{U}{2} + \frac{U}{2}\kappa - \epsilon & d_x - id_y \\ d_x + id_y & -d_z + \frac{U}{2} - \frac{U}{2}\kappa - \epsilon \end{vmatrix} = 0, \quad (7)$$

we obtain

$$\begin{aligned} f(\epsilon) &= \epsilon^4 - 3U\epsilon^3 + \left(\frac{13}{4}U^2 - d_z^2 - d_x^2 - d_y^2\right)\epsilon^2 \\ &+ (Ud_z^2 + 2U(d_x^2 + d_y^2) - \frac{3}{2}U^3)\epsilon \\ &+ \frac{U^4}{4} - \frac{U^2 d_z^2}{4} - U^2(d_x^2 + d_y^2) = 0, \end{aligned} \quad (8)$$

Solving this equation, we can find three different types of degenerate eigenvalues called degenerate points. The I-type degenerate point is  $\epsilon = U/2$  when  $d_x^2 + d_y^2 = 0$ , the II-type degenerate point is  $\epsilon = U$  when  $d_z = 0$ , and the III-type degenerate point can be obtained by setting  $d_z = \pm \frac{1}{2}\{U^{\frac{2}{3}} - [4(d_x^2 + d_y^2)]^{\frac{1}{3}}\}^{\frac{3}{2}}$ .  $f(\epsilon) = 0$  leads to,

$$\begin{aligned} \{2(\epsilon - \frac{U}{2}) - [4U(d_x^2 + d_y^2)]^{\frac{1}{3}}\}^2 \{4(\epsilon - \frac{U}{2})^2 \\ + [-4U + 4[4U(d_x^2 + d_y^2)]^{\frac{1}{3}}](\epsilon - \frac{U}{2}) \\ - U[4U(d_x^2 + d_y^2)]^{\frac{1}{3}}\} = 0, \end{aligned} \quad (9)$$

where the III-type degenerate point is at

$$\epsilon = \frac{U}{2} + \frac{1}{2}[4U(d_x^2 + d_y^2)]^{\frac{1}{3}}. \quad (10)$$

In the following, we would examine these eigenvalues and show that bifurcation appears around these degenerate points. This means that additional eigenvalues in nonlinear Hamiltonian would appear. This is why nonlinear systems possess new Bloch band structures that are completely different from their linear counterparts.

Before proceeding to analyze the three types of degenerate eigenvalues, we approximate nonlinear Bloch Hamiltonian around the degenerate points by using Taylor expansions, which leads to a correction of  $\epsilon^{(1)}$  to the eigenvalue  $\epsilon^{(0)}$  up to the first order in the deviation from the degenerate points. The first-order correction  $\epsilon^{(1)}$  is given by

$$a(\epsilon^{(1)})^2 + b\epsilon^{(1)} + c = 0, \quad (11)$$

where

$$\begin{aligned} a &= \frac{1}{2} \left( \frac{\partial^2 f(\epsilon)}{\partial \epsilon^2} \right)^{(0)}, \\ b &= \left( \frac{\partial f(\epsilon)}{\partial \epsilon} \right)^{(0)} + \left( \frac{\partial^2 f(\epsilon)}{\partial \epsilon \partial d_\mu} \right)^{(0)} d_\mu^{(1)}, \\ c &= \left( \frac{\partial f(\epsilon)}{\partial d_\mu} \right)^{(0)} d_\mu^{(1)} + \frac{1}{2} \left( \frac{\partial^2 f(\epsilon)}{\partial d_\nu \partial d_\mu} \right)^{(0)} d_\nu^{(1)} d_\mu^{(1)}. \end{aligned} \quad (12)$$

Here  $()^{(0),(1)}$  denotes the zero-order or first-order values, which is parameter dependent. Generally, this parameter is wavevector  $\mathbf{k}$  in the momentum space, thus the zero-order or first-order values at  $\mathbf{k} = \mathbf{k}_0$  can be given by  $d_\mu^{(0)} = d_\mu(\mathbf{k})|_{\mathbf{k}=\mathbf{k}_0}$ ,  $d_\mu^{(1)} = (\mathbf{k} - \mathbf{k}_0) \cdot \partial_{\mathbf{k}} d_\mu(\mathbf{k})|_{\mathbf{k}=\mathbf{k}_0}$ ,  $\mu = x, y, z$  and  $f(\epsilon)$  is given in Eq. (8). The values of  $b^2 - 4ac$  can be regarded as a critical condition for the appearance of bifurcation.

Consider the I-type degenerate point  $\epsilon^{(0)} = U/2$  and  $d_x^{(0)} = 0, d_y^{(0)} = 0, \epsilon^{(1)}$  is given by

$$\epsilon^{(1)} = \pm \frac{U \sqrt{(d_x^{(1)})^2 + (d_y^{(1)})^2}}{\sqrt{U^2 - 4(d_z^{(0)})^2}}. \quad (13)$$

From the last equation, it is easy to find that if  $U_c \neq 2|d_z^{(0)}|$ ,  $\epsilon^{(1)}$  would get two values, then  $U_c = 2|d_z^{(0)}|$  can be treated as the critical condition for bifurcation.

Around the II-type degenerate point  $\epsilon^{(0)} = U$  with  $d_z^{(0)} = 0, \epsilon^{(1)}$  is given by

$$\epsilon^{(1)} = \pm \frac{U}{2\sqrt{2}\sqrt{U^2 - 4((d_x^{(0)})^2 + (d_y^{(0)})^2)}}. \quad (14)$$

Similarly,  $U_c = 2\sqrt{(d_x^{(0)})^2 + (d_y^{(0)})^2}$  is the critical condition for bifurcation. Critically, the III-type degenerate point is connected to the closing of gap between different Bloch bands, we will perform detailed discussion in the following sections.

### III. BLOCH BAND STRUCTURES IN NONLINEAR CHERN INSULATOR

In this section, we analyze Bloch band structures in momentum space focusing our attention on Bloch form of nonlinear Hamiltonians. We introduce a simple nonlinear system by adding the Kerr-type nonlinearity into the Chern insulator model. The dynamics of such a system in terms of Bloch form of wave eigenfunctions is governed by

$$i\partial_t \Psi(\mathbf{k}, t) = \hat{H}(\mathbf{k}, t) \Psi(\mathbf{k}, t), \quad (15)$$

where the wave vector  $\mathbf{k} = (k_x, k_y)$  is restricted to  $k_{x,y} \in [0, 2\pi]$  called the restricted Brillouin zone. Consider a two-band model and write  $\Psi(\mathbf{k}, t) = [\psi_1(\mathbf{k}, t), \psi_2(\mathbf{k}, t)]^T$  and  $\hat{H}(\mathbf{k}, t) = \hat{H}_L(\mathbf{k}) + \hat{H}_{NL}(\mathbf{k}, t)$ .  $\hat{H}_L(\mathbf{k})$  and  $\hat{H}_{NL}(\mathbf{k})$  are linear and nonlinear parts of the Bloch Hamiltonian

$$\begin{aligned} \hat{H}_L(\mathbf{k}) &= d_x(\mathbf{k})\sigma_x + d_y(\mathbf{k})\sigma_y + d_z(\mathbf{k})\sigma_z, \\ \hat{H}_{NL}(\mathbf{k}) &= U[|\psi_1(\mathbf{k}, t)|^2, 0; 0, |\psi_2(\mathbf{k}, t)|^2], \end{aligned} \quad (16)$$

with

$$\begin{aligned} \mathbf{d}(\mathbf{k}) &= (d_x(\mathbf{k}), d_y(\mathbf{k}), d_z(\mathbf{k})) \\ &= (J \sin k_x, J \sin k_y, u + J \cos k_x + J \cos k_y), \end{aligned} \quad (17)$$

where  $u$  is a topological parameter that can change the topological phases and  $U$  is nonlinear strength. Throughout this manuscript, we set  $J = 1$  and take  $J$  as the units of energy and  $1/J$  as the units of time.

In order to obtain Bloch band structures, we consider the stationary solution  $\Psi(\mathbf{k}, t) = e^{-i\epsilon t} \Phi(\mathbf{k})$  to the Schrödinger equation. The time-independent eigenvalue equation is given by

$$\hat{H}(\mathbf{k}) \Phi(\mathbf{k}) = \epsilon \Phi(\mathbf{k}). \quad (18)$$

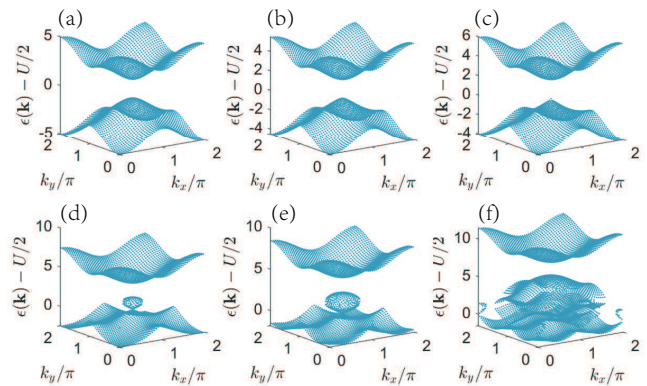


FIG. 1: Bloch band structures in the topological trivial regime  $u = 3$  with different  $U$  as in (a)  $U = 0$ , (b)  $U = 1$ , (c)  $U = 2$ , (d)  $U = 5$ , (e)  $U = 7$ , and (f)  $U = 13$ .

#### A. Linear regime

We first consider Bloch band structures in linear Bloch Hamiltonian. When  $U = 0$ , Bloch Hamiltonian  $\hat{H}(\mathbf{k})$  is  $\hat{H}_L(\mathbf{k})$  and eigenvalues of  $\hat{H}_L(\mathbf{k})$  are

$$\epsilon_{\pm} = \pm \sqrt{u^2 + 2 + 2u \cos k_x + 2u \cos k_y + 2 \cos k_x \cos k_y}.$$

There is an energy gap between these two Bloch bands. And the energy gap is closed when  $u = 0, \pm 2$  at the special points in  $\mathbf{k}$  space. These points are the so-called Dirac points. Since we consider linear Bloch bands, we can characterize different topology of band by Chern number defined as  $C = \frac{1}{2} \text{sgn}(u+2) + \frac{1}{2} \text{sgn}(u-2) - \text{sgn}(u)$ . Thus, different values of  $u$  would correspond to different topology of Bloch bands[86].

#### B. Nonlinear regime

Now, we turn to the nonlinear Bloch Hamiltonian. Unlike linear Bloch Hamiltonian, we can not use Chern number to distinguish different topological phases due to appearance of degenerate points in Bloch band. Nevertheless, we can still continue to discuss Bloch band structures because they are different from linear one. With Eq. (8) and some elaborate algebra, a  $\mathbf{k}$ -dependent algebraic equation for eigenvalues  $\epsilon$  can be given

$$\begin{aligned} \epsilon^4(\mathbf{k}) &- 3U\epsilon^3(\mathbf{k}) + \left[\frac{13}{4}U^2 - d_z^2(\mathbf{k}) - d_x^2(\mathbf{k}) - d_y^2(\mathbf{k})\right]\epsilon^2(\mathbf{k}) \\ &+ [Ud_z^2(\mathbf{k}) + 2U(d_x^2(\mathbf{k}) + d_y^2(\mathbf{k})) - \frac{3}{2}U^3]\epsilon(\mathbf{k}) \\ &+ \frac{U^4}{4} - \frac{U^2 d_z^2(\mathbf{k})}{4} - U^2(d_x^2(\mathbf{k}) + d_y^2(\mathbf{k})) = 0. \end{aligned} \quad (19)$$

In the following, we tune nonlinear strength  $U$  and topological parameter  $u$  to show different band structures.

We first consider topological trivial case, i.e.  $u > 2$ . In Fig. 1, we plot several Bloch band structures with

different nonlinear strength  $U$  and fixed  $u = 3$  as well as  $d_x(\mathbf{k}) = d_y(\mathbf{k}) = 0$ . The I-type degenerate points can be easily found. Using the critical condition of the I-type degenerate point given in the last section, we obtain the critical nonlinear strength,  $U_c = 2|u + 2|, 2|u|, 2|u|, 2|u - 2|$ . For  $u = 3$  in the trivial regime, critical nonlinear strength are  $U_c = 10, 6, 6, 2$ . When  $U < U_c$ , as shown in Fig. 1(a)-(c), with  $U$  increasing, Bloch band structures start to change, see Fig. 1(d). Cone structures can be formed, which are regarded as nonlinear Dirac cones[81]. Tap between different Bloch bands exists permanently with increasing  $U$ , which is different from the topological nontrivial regime, see Fig. 1(f). It is worth noting that in topological trivial regime, we cannot obtain the II-type degenerate points because the condition  $d_z(\mathbf{k}) = u + \cos k_x + \cos k_y = 0$  cannot be satisfied.

In topological nontrivial regime, we set the topological parameter  $u = 1.2$  and  $U = 0, 1, 1.6, 2.4, 3, 9$  was chosen to discuss the problem. In this case,  $U_c = 2|u + 2|, 2|u|, 2|u|, 2|u - 2| = 6.4, 2.4, 2.4, 1.6$ . By  $u + \cos k_{x_0} + \cos k_{y_0} = 0$  and  $d_z(\mathbf{k}) = 0$ , we can obtain the corresponding II-type degenerate points in the upper band. Using the critical condition of the II-type degenerate point in the last section, we can give the corresponding critical nonlinear strength  $U_c = 2\sqrt{(\sin k_{x_0})^2 + (\sin k_{y_0})^2}$ . When  $U < U_c$ , as shown in Fig. 2(a)-(c), Bloch band structure remain unchanged. As  $U$  increases, eigenvalues in the vicinity of the I-type degenerate points in the lower band become sharper, see Fig. 2(c). The other cone structures in the lower band and tubed structures in the upper band can be found in Fig. 2(d)-(e). And gap between different Bloch bands disappears with increasing  $U$ , as shown in Fig. 2(f).

Besides, using  $d_z(\mathbf{k}) = \pm \frac{1}{2} \{ U^{\frac{2}{3}} - [4(d_x^2(\mathbf{k}) + d_y^2(\mathbf{k}))]^{\frac{1}{3}} \}^{\frac{3}{2}}$ , III-type degenerate points can be found at the inner and outer edges of cone structure and tubed structure. In particular, the nonlinear strength  $U$  and topological parameter  $u$  that makes the Bloch band gaps closed can be given by the III-type degenerate points. And tubed structure in the excited Bloch band and cone structure in the ground Bloch band merge gradually into one continued Bloch band without gap, as shown in Fig. 2(f), which we will give details in the next section by the virtue of effective nonlinear Hamiltonian.

To simplify the discussion, although the cone structures and tubed structures form in two-dimensional momentum space, we will use the one-dimensional view of these structures to explain dynamics of nonlinear systems and nonlinear Bloch band in the following section. Thus, cone structures and tubed structures in one-dimension is of loop.

### C. Analysis on gap closing in trivial and nontrivial topological regime

In this section, we discuss gap closing at different values of parameters via III-type degenerate point. Linear

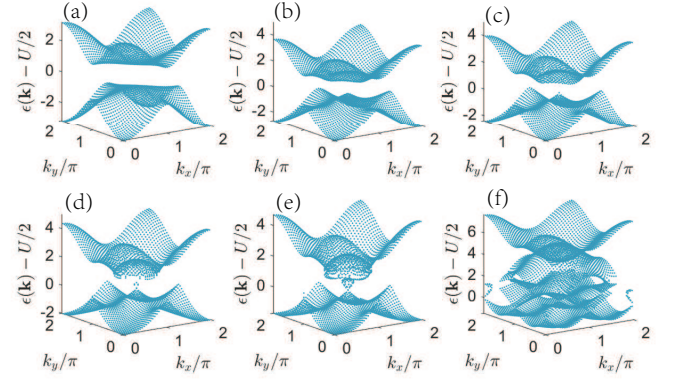


FIG. 2: Bloch band structures in topological nontrivial regime  $u = 1.2$ . With increasing  $U$  in (a)  $U = 0$ , (b)  $U = 1$ , (c)  $U = 1.6$ , (d)  $U = 2.4$ , (e)  $U = 3$ , (f)  $U = 9$ .

Hamiltonian have an energy gap in the insulator regime. With tuning the parameter, energy gap can be closed and reopened. Based on Bloch band structures in nonlinear system above, gap between different Bloch bands with increasing  $U$  in topological nontrivial regime, as shown in Fig. 2(f)-(h), can be closed and cannot be reopened anymore, while gap in topological trivial regime remain opened with increasing  $U$ , as shown in Fig. 2(e). In contrast to gap closing in linear Hamiltonian, here we show the gap closing between different Bloch bands in nonlinear systems by tuning nonlinear strength  $U$  and topological parameter  $u$ . For the sake of concise expression, here we use the effective Hamiltonian of the nonlinear Chern insulator model(Eq. (16)) in the vicinity of  $\mathbf{k} = (\pi, \pi)$  to illustrate the gap

$$\begin{aligned} \hat{H}_{eff} = & (-p_x)\sigma_x + (-p_y)\sigma_y + p_z\sigma_z \\ & + U[|\phi_1(\mathbf{p})|^2, 0; 0, |\phi_2(\mathbf{p})|^2], \end{aligned} \quad (20)$$

where  $p_z = u - 2 + \frac{1}{2}(p_x^2 + p_y^2)$ ,  $p_x = k_x - \pi$ , and  $p_y = k_y - \pi$ , then we get  $\mathbf{p}$ -dependent algebraic eigenvalue equation for  $\epsilon$  via the effective Hamiltonian

$$\begin{aligned} (\epsilon(\mathbf{p}) - U)^2 [(\epsilon(\mathbf{p}) - U/2)^2 - p_x^2 - p_y^2] \\ - p_z^2 (\epsilon(\mathbf{p}) - U/2)^2 = 0. \end{aligned} \quad (21)$$

Note that different Bloch band structures would be given by different topological parameter  $u$  and nonlinear strength  $U$ .

In Fig. 3, we show the Bloch band structures calculated by effective Hamiltonian. In contrast to original nonlinear Bloch Hamiltonian, Bloch band obtained by the effective Hamiltonian would be more simple, and tubed structure would appear around the circle  $p_x^2 + p_y^2 = 4 - 2u$ . This structure is clearly shown in Fig. 3(i), which can be produced by rotating the Fig. 3(f) around the axis of  $p = 0$ . Considering the topological nontrivial regime  $u = 1$  with

nonlinear strength  $U = 4$  as shown in Fig. 3(f), the Bloch band would produce looped structure in the excited Bloch band and the ground band jointly. Here we only show the cross-section  $p_x = p_y = p$  of Bloch band.

We tune  $u$  with fixed  $U = 4$ . When  $u \approx 1.066$ , gap between different Bloch bands closes, as shown in Fig. 3(a), and the three looped structures in the lower and upper band merge into a Bloch band. After that, when  $u = 1.1$ , as shown in Fig. 3(b), these structures form a new large looped structure, and the excited Bloch band and ground Bloch band overlap. Next looped structure deforms with increasing  $u$ , as shown in Fig. 3(b)-(d). In Fig. 3(d), the looped structure from the ground Bloch band is attached to the excited Bloch band so that gap between them close. After that, the gap starts to reopen, like the gap between Bloch bands with  $u = 3$  in Fig. 3(e). Here we show the range of the topological parameter  $u$  that makes gap closed is  $u \approx [1.066, 2]$ .

Alternatively, we tune  $U$  with fixed  $u = 1$ , where we see the gap opened in topological trivial regime permanently. After  $U = 4$  in Fig. 3(f), the three looped structures approach to each other, as shown in Fig. 3(g), which is similar to Fig. 3(a). Then gap closing can be observed between the two enlarged Bloch band structures, as shown in Fig. 3(j)-(k). After that, a new looped structure can be formed[see Fig. 3(h)], which is similar to Fig. 3(b).

At the III-type degenerate point, critical  $U$  and  $u$  that make gap closed can be found numerically via  $d_z(\mathbf{p}) = -\frac{1}{2}\{U^{\frac{2}{3}} - [4(d_x^2(\mathbf{p}) + d_y^2(\mathbf{p}))^{\frac{1}{3}}]^{\frac{3}{2}}\}^{\frac{3}{2}}$ . With the effective Hamiltonian, the algebraic equation can be given by

$$[u - 2 + \frac{1}{2}(p_x^2 + p_y^2)] = -\frac{1}{2}\{U^{\frac{2}{3}} - [4(p_x^2 + p_y^2)^{\frac{1}{3}}]^{\frac{3}{2}}\}^{\frac{3}{2}}, \quad (22)$$

where  $p_x = p_y = p$  is specified. From this equation we can find that III-type degenerate points satisfy  $\epsilon(-p) = \epsilon(p)$ . There are in general four different  $p$  in quasimomentum space and four corresponding III-type twofold degenerate points  $\epsilon(p)$ . In particular, only two different  $p$  and two corresponding III-type twofold degenerate points can be given numerically by careful choices of  $U$  and  $u$ . This indicates that two III-type twofold degenerate points merge into a III-type twofold degenerate points so that gap between different bands disappear, see Fig. 3(a). Thus critical  $U$  and  $u$  for gap closing can be specified numerically. In Fig. 3(a), two different  $p$  and two corresponding III-type twofold degenerate points can be given numerically with  $u \approx 1.066$  and  $U = 4$ . In Fig. 3(g),(j)-(k), we find that two different  $p$  and two corresponding III-type twofold degenerate points can be given numerically when  $u = 1$  and  $U_g \approx 4.1996$ , falling exactly in the range  $U_g \in [4.1993, 4.1997]$  (see Fig. 3(j)-(k)). In addition, manipulating  $u$ , we can also tune additional parameter  $U$  to close the gap.

#### IV. LINEAR RESPONSE OF NONLINEAR CHERN INSULATOR TO EXTERNAL FIELD

To investigate the linear response of nonlinear Chern insulator, we examine the dynamics of the nonlinear Chern insulator discussed above driven by external field  $F$ . We first consider the time-dependent nonlinear Bloch Hamiltonian  $\hat{H}(t) = H(\mathbf{k}(t))$ , the corresponding wave vector given by  $\mathbf{k} = [k_x, k_y(t)]$  and external field  $F$  can be introduced by  $k_y(t) = k_{y0} + Ft$ . Initially, consider the nonlinear eigenstate  $|\Psi_n^{NL}(t)\rangle$  at  $t = 0$  in a given Bloch band, and then the expectation of non-vanishing velocity  $\hat{v}_x(k_x, k_y(t)) = \frac{1}{\hbar}\partial_{k_x}\hat{H}(t)$  with time-dependent density matrix can be calculated numerically by

$$\begin{aligned} v_n^x(k_x, k_y(t)) &= \langle \Psi(t) | \hat{v}_x(k_x, k_y(t)) | \Psi(t) \rangle \\ &= \frac{1}{\hbar} \text{tr}[\hat{\rho}(t)\partial_{k_x}\hat{H}(t)], \end{aligned} \quad (23)$$

where  $n = 1, 2$  denotes ground Bloch band or excited Bloch band and  $\hat{\rho}(t)$  denotes the time-dependent density operator. Then we use  $k_y(t) = k_{y0} + Ft$  to obtain  $\partial_t = F\partial_{k_y}$ , and then we consider ground Bloch band and excited Bloch band respectively. The current in a complete Bloch band is given by

$$J_n^x = \sum_{k_x, k_y} v_n^x(k_x, k_y(t)). \quad (24)$$

And the current[87] is given by

$$J_n^x = \sigma_{xy}F, \quad (25)$$

where  $\sigma_{xy}$  is the linear response of this nonlinear Chern insulator

$$\sigma_{xy} = \frac{1}{F} \sum_{k_x, k_y} v_n^x(k_x, k_y(t)) = \frac{\nu^{NL}}{\hbar}, \quad (26)$$

where  $\nu^{NL}$  is a quantized number modified by nonlinearity, which imply that quantized response of nonlinear systems could be broken. Consider the Bloch band structures of nonlinear Chern insulator in Sec.III, we show the diagram with different parameters  $u$  and  $U$ , based on whether cone structures and tubed structures appear. In Fig. 4(a) and (b), there are two regions, one of which is adiabatic region(A) and the other is non-adiabatic(nA) region, which are linked to adiabaticity of nonlinear systems. In linear regime, we give a quantized response with different parameter  $u$ , as shown by the red line in Fig. 4. Nevertheless, in nonlinear regime, combining linear response with the nonlinear Bloch band structures, there are two kinds of linear response, one of which is non-quantized response modified by nonlinearity, as shown in Fig. 4(c1) and (d1), while the other type of the linear response can be broken completely and generate the drastic change deviate from quantized response, as shown in Fig. 4(c2) and (d2). And then these two different kinds of destruction of quantized linear response correspond

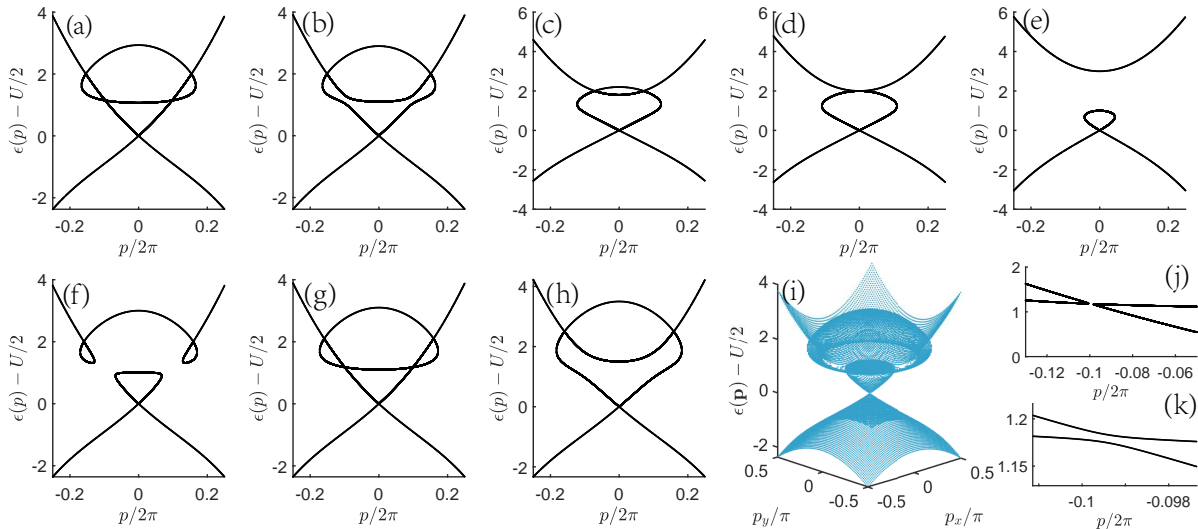


FIG. 3: Bloch band structures in effective Hamiltonian with different topological parameter  $u$  and nonlinear strength  $U$ , and fixed  $p_x = p_y = p$ . In the upper panel we give the structures based on increasing  $u$  and fixed  $U = 4$  in (a)  $u = 1.066$ , (b)  $u = 1.1$ , (c)  $u = 1.8$ , (d)  $u = 2$ , and (e)  $u = 3$ . In the lower panel we give the structures with increasing  $U$  (f)  $U = 4$ , (g)  $U = 4.2$ , and (h)  $U = 5$  where we use fixed  $u = 1$ , and meanwhile we give gap closing point between nonlinear strength (j)  $U = 4.1993$  and (k)  $U = 4.1997$ . And we give Bloch bands with varied  $p_x$  and  $p_y$  in (i)  $u = 1, U = 4$ .

to the two regions of the diagram in Fig. 4(a) and (b). What happens to linear response of nonlinear systems to external field? Because adiabatic evolution in nonlinear systems is broken due to the appearance of new structures. This question can be tackled and shown using numerical simulations of dynamics of nonlinear systems. In the following section, for the sake of simplicity, we will choose one of the adiabatic evolution paths to show the dynamics of nonlinear systems and the failure of adiabatic evolution due to the new structure.

## V. ADIABATIC EVOLUTION OF NONLINEAR CHERN INSULATOR

As a result of the appearance of the new structures, dynamics of nonlinear systems is not trivial anymore. In the previous studies, authors shown that the adiabatic evolution would be broken when the system arrives at the tail of loop structure[61, 62, 73]. In this section, we explore this problem again but for our topological systems. For simplicity, we start with considering an evolution path in  $k_x = k_y$  direction. Considering that  $\mathbf{k}$  in quasimomentum increases from  $(k_x, k_y) = (0, 0)$  to  $(k_x, k_y) = (2\pi, 2\pi)$ , time evolution state is initially prepared in the eigenstate of nonlinear Hamiltonian at quasimomentum  $(k_x, k_y) = (0, 0)$  and then evolves governed by Eq. (15) with  $\mathbf{k} = \mathbf{F}t + \mathbf{k}_0$  and  $\mathbf{k}_0 = 0$ , where a very weak constant acceleration force  $\mathbf{F}$  is given by  $\mathbf{F} = (F_x, F_y) = (F, F)$ . This force is equivalent to external field in the last section.

### A. dynamics of nonlinear Chern insulator

Here we consider acceleration force  $F_x = F_y = F$ . Along the path, looped structures can be obtained from the nonlinear Bloch band structures. We address the probability  $|\Psi_i(t)|^2, i = 1, 2$  obtained from the time evolution state  $\Psi(t) = [\Psi_1(t), \Psi_2(t)]^T$ . Firstly, consider the topological nontrivial regime, the probability  $|\Psi_i(t)|^2, i = 1, 2$  evolves adiabatically from instantaneous eigenstate of the ground Bloch band at  $k = 0$ , and then there is an irregular oscillation around the I-type degenerate point due to looped structure in the ground Bloch band, as shown in Fig. 5(a) and (e1). Then using eigenstate from the excited Bloch band at  $k = 0$  as an initial state, we show the time evolution in Fig. 5(c), and band structure in Fig. 5(g1). We can observed that the excited Bloch band produce a looped structure, and there is an irregular oscillation at the tail of looped structure from the excited Bloch band.

In topological trivial regime, one looped structure is produced at the ground Bloch band, as shown in Fig. 5(b), (d) and (h1). And the initial state in Fig. 5(b) and (d) is set to be the eigenstate from ground Bloch band at  $k = 0$  and the eigenstate from excited Bloch band at  $k = 0$ , respectively. Here irregular oscillation in the ground Bloch band appear around the I-type degenerate point, as shown in Fig. 5(b). Whereas in the excited Bloch band, looped structure cannot be produced so that there is not irregular oscillation along the path. This indicates that adiabatic evolution is satisfied, as shown in Fig. 5(d).

In short, the presence of nonlinearity induced novel structures alter the time evolution dynamics and the adi-

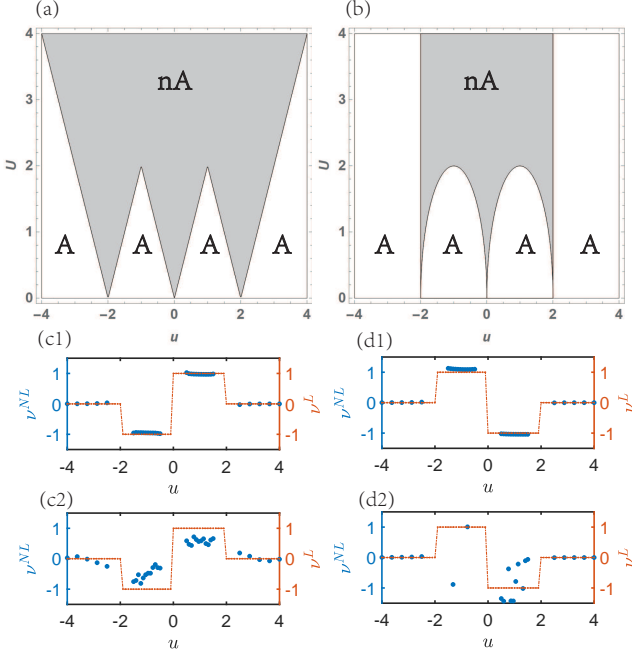


FIG. 4: Linear response of nonlinear system to external field  $F = 0.01$ . (a) and (b) show diagrams with parameter  $u$  and  $U$  in ground Bloch band and excited Bloch band respectively, where white region denotes adiabatic evolution(A), and gray region denotes non-adiabatic evolution(nA). Dashed lines in (c1), (c2), (d1) and (d2) denote linear response of linear Chern insulator, and  $\nu^L$  on the right side denotes quantized number. Blue Points denote linear response in nonlinear Chern insulator, and  $\nu^{NL}$  on the left side denote nonlinear modified quantized number. At last, nonlinear strength  $U$  are  $U = 0.5$  in (c1) and (d1), and  $U = 3$  in (c2) and (d2).

adiabaticity breaks down in the nonlinear Chern insulator. This leads to non-adiabatic time evolutions and consequently the linear response to external fields changes drastically, as shown in Fig. 4(c2) and (d2). On the contrary, the adiabatic evolution would give quantized linear responses, as shown in Fig. 4(c1) and (d1).

### B. average energy and adiabaticity

In order to calculate the expectation value of the time-dependent nonlinear Hamiltonian, we compute numerically the wave function at time  $t$  by solving  $i\hbar\partial_t\Psi(t) = \hat{H}(t)\Psi(t)$ . Substituting the wave function  $|\Psi(t)\rangle$  into,  $\epsilon(t) = \langle\Psi(t)|\hat{H}(t)|\Psi(t)\rangle$ , the expectation of the Hamiltonian will be given. With different parameters, we find different structures (see Fig. 5(e1)-(h1)) and different time evolution of average  $\epsilon(t)$ . When  $u < 2$ , namely in non-trivial regime,  $\epsilon(t)$  starts oscillating around the I-type degenerate point as shown in Fig. 5(e1)-(e2), while it starts oscillating at the tail of the looped structure in the excited Bloch band, see Fig.5(g1). The simulation was performed with the same initial states as in the last section.

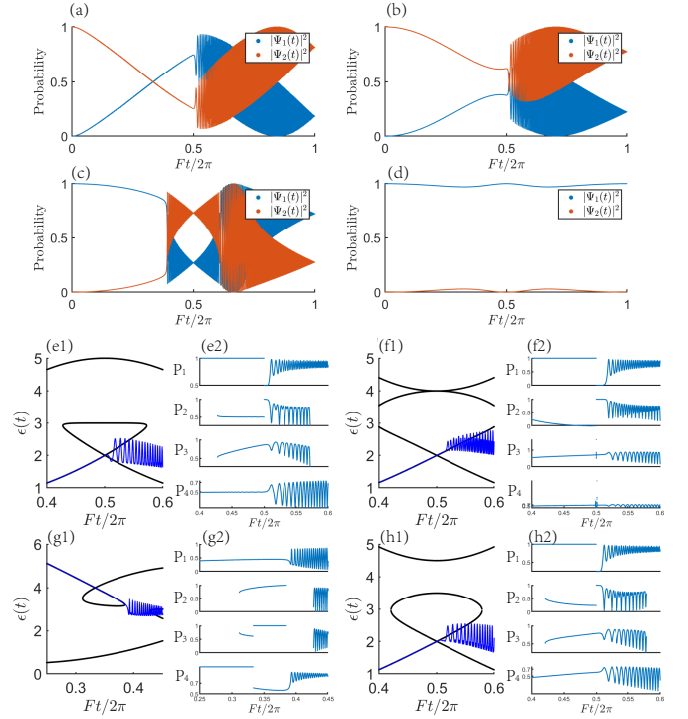


FIG. 5: Time evolution, dynamical energy level, and transition probability between the resulting state and the instantaneous eigenstates with different parameters and  $k_x = k_y = k = Ft$ . To calculate the time evolution, we set acceleration force  $F = 0.01$  and nonlinear strength  $U = 4$ . In (a)-(d), time-dependent probability with different initial states, eigenstate at  $k = 0$  in the ground Bloch band is set as the initial state in (a) and (c), and eigenstate at  $k = 0$  in the excited Bloch band is set as the initial state in (b) and (d). The other parameters chosen are (a)  $u = 1$ , (b)  $u = 1$ , (c)  $u = 2.5$ , and (d)  $u = 2.5$ . Here we show four different Bloch band structures and the corresponding transition probability in (e1)  $u = 1$ , (f1)  $u = 2$ , (g1)  $u = 1$  and (h1)  $u = 2.5$ . In (e1), (f1), and (h1), initial state is eigenstate at  $k = 0$  in the ground Bloch band, and initial state is eigenstate at  $k = 0$  in the excited Bloch band in (g1). For comparison, the local features of complete evolution process are also shown.

We also find that when  $u > 2$  (see Fig. 5(h1)), irregular oscillations in  $\epsilon(t)$  start around the I-type degenerate points, this is the same as  $\epsilon(t)$  in the nontrivial regime that gets start from the ground instantaneous eigenstate at  $k = 0$ . When  $u = 2$  (see Fig. 5(f1)), we find that irregular oscillations in  $\epsilon(t)$  start behind the appearance of degenerate point. Namely, the oscillations start at a value larger than that at which the degenerate point occurs. In other words, irregular oscillations appear around the degenerate point, not exactly at the point. In particular, at the critical point  $u = 2$ , the distance between the location of irregular oscillation and the degenerate point is the largest one.

In the following, we would use the populations on each instantaneous bands to quantify the adiabaticity. To obtain the transition probability, a set of  $\mathbf{k}$ -dependent

eigenstates  $\chi(\mathbf{k})$  of nonlinear Bloch Hamiltonian can be given by Eq. (18) and then instantaneous eigenstates  $\chi_i(\mathbf{k}(t))$  is obtained. And transition probability can be define as,  $P_i = |\chi_i(\mathbf{k}(t))^\dagger \Psi(\mathbf{k}(t))|^2$ . Generally speaking, these nonlinear instantaneous eigenstates cannot be orthogonality and sum of these transition probability will not be unity. There are some details on instantannoues eigenstates in Appendix. A. Using the transition probability  $P_i = |\chi_i^\dagger(\mathbf{k})\Psi(\mathbf{k}(t))|^2$ , the difference between evolution state and instantaneous eigenstates are shown in Fig. 3(e2)-(h2). The transition probability  $P_1 - P_4$  correspond to the instantaneous eigenstates with eigenvalues from small to large. When  $P_i$  is unity which imply that evolution state is the same as nonlinear instantaneous eigenstates, adiabatic evolution is satisfied, and while transition probability is irregular oscillation which implies that these two states are different from each other, adiabatic evolution is broken.

## VI. CONCLUSIONS

In summary, the Bloch band structures and gap closing has been discussed for generalized Chern insulator described by a nonlinear Hamiltonian. In contrast to linear systems, Bloch band in nonlinear systems possesses additional structures around degenerate points determined by the competition between the nonlinearity and other parameters of the system. The observed features are completely different from that in linear systems. For example, in nonlinear Chern insulator, cone structure from the ground Bloch band and tubed structure from the excited Bloch band appear. From the other aspect, the linear response of the system to external fields is also different from the linear one. Namely, the response is not quantized due to nonlinearity. To explain this feature, we examine the adiabaticity of the time evolution and find that in non-adiabatic regime, irregular oscillations appear around the center of the cone or the tail of the tube of the energy bands. Experimentally, band structures and tunneling probabilities in nonlinear systems can be observed in ultracold atoms in a moving one-dimensional optical lattice[73]. Alternatively, it is also realizable in nonlinear circuit arrays, which can be constructed by setting one-dimensional transmission-line circuits in electronic systems[75]. Strong nonlinear regime can be realized in a one-dimensional mechanical Su-Schrieffer-Heeger interface model with nonlinearity[74]. Finally, our method to describe Bloch band structures in nonlinear systems can be extended to other nonlinear topological systems, for example high dimensional systems and systems with different nonlinear strength. We conjecture that pursuing these interesting band structures in topological systems with nonlinearity would be the main concern in future works.

## Acknowledgments

We thank Hongzhi Shen and Dexiu Qiu for helpful discussions. This research was funded by National Natural Science Foundation of China (NSFC) under Grants No. 12175033 and No. 12147206, and National Key R&D Program of China(No.2021YFE0193500).

## Appendix A: Eigenstates of nonlinear Bloch Hamiltonian

### 1. Non-degenerate regime

By virtue of nonlinear Bloch Hamiltonian, eigenstates can be obtained. Here we assume that these eigenvectors are normalized, but generally speaking, they are not orthogonal to each other due to nonlinearity. Nonlinear Bloch Hamiltonian is given by

$$H(\mathbf{k}) = \frac{U}{2}\sigma_0 + d_x(\mathbf{k})\sigma_x + d_y(\mathbf{k})\sigma_y + d_z^{NL}(\mathbf{k})\sigma_z \quad (\text{A1})$$

where  $d_z^{NL}(\mathbf{k}) = d_z(\mathbf{k})\left(\frac{2\epsilon(\mathbf{k})-U}{2(\epsilon(\mathbf{k})-U)}\right)$ , specially, when  $U = 0$ , it will be  $d_z^{NL}(\mathbf{k}) = d_z(\mathbf{k})$ . And eigenstate(omitting  $\mathbf{k}$  for simplicity) is given by

$$\chi = \frac{1}{\sqrt{2(\epsilon - \frac{U}{2})(\epsilon - \frac{U}{2} - d_z^{NL})}} \begin{pmatrix} d_x - id_y \\ \epsilon - \frac{U}{2} - d_z^{NL} \end{pmatrix}, \quad (\text{A2})$$

where  $\chi = [\chi_1, \chi_2]^T$ , and we get general eigenstates in nonlinear systems, but we need to make detailed discussion about the eigenstates of degenerate eigenvalues.

### 2. Degenerate regime

There are three kinds of eigenstates for the three types of degenerate points. Consider  $d_x^2 + d_y^2 = 0, \epsilon = U/2$ , namely, I-type degenerate point, and use the expression of  $|\chi_1|^2, |\chi_2|^2$  given in the main manuscript, then substitute  $\epsilon$  into  $|\chi_1|^2, |\chi_2|^2$ , and eigenstates of the I-type degenerate point is given by

$$\chi_{d_x^2+d_y^2=0} = \begin{pmatrix} \sqrt{\frac{1}{2} + \frac{d_z}{2(\epsilon-U)}} e^{i\theta} \\ \pm \sqrt{\frac{1}{2} - \frac{d_z}{2(\epsilon-U)}} \end{pmatrix}, \quad (\text{A3})$$

where  $\theta$  are arbitrary phase depending on which direction we approach the degenerate point.

Consider  $d_z = 0, \epsilon = U$ , namely, II-type degenerate point,  $d_z^{NL}$  is given by

$$d_z^{NL} = d_z + \frac{\kappa}{2} \quad (\text{A4})$$

where  $d_z^{NL}$  is  $\kappa$ -dependent which is considered in the main manuscript, and corresponding  $(\kappa, \epsilon) = (\pm \frac{\sqrt{U^2 - 4(d_x^2 + d_y^2)}}{U}, U)$ , and then substitute  $\kappa, \epsilon$  into  $d_z^{NL}$ , and eigenstates of the II-type degenerate point is given by

$$\chi_{d_z=0} = \frac{1}{\sqrt{2(\epsilon - \frac{U}{2})(\epsilon - \frac{U}{2} - \frac{\kappa}{2})}} \begin{pmatrix} d_x - id_y \\ \epsilon - \frac{U}{2} - \frac{\kappa}{2} \end{pmatrix}. \quad (\text{A5})$$

Consider  $d_z = \pm \frac{1}{2} \{U^{\frac{2}{3}} - [4(d_x^2 + d_y^2)]^{\frac{1}{3}}\}^{\frac{3}{2}}$ ,  $\epsilon = U/2 + 1/2[4U(d_x^2 + d_y^2)]^{\frac{1}{3}}$ , namely, III-type degenerate point, eigenstate is given by the form of eigenstates in Eq. A3.

- 
- [1] D. J. Thouless, M. Kohmoto, M. P. Nightingale, and M. den Nijs, quantized Hall conductance in a two-dimensional periodic potential, *Phys. Rev. Lett.* 49, 405 (1982).
- [2] K. von Klitzing, The quantized Hall effect, *Rev. Mod. Phys.* 58, 519 (1986).
- [3] M. Z. Hasan and C. L. Kane, Colloquium: Topological insulators, *Rev. Mod. Phys.* 82, 3045 (2010).
- [4] X.-L. Qi and S.-C. Zhang, Topological insulators and superconductors, *Rev. Mod. Phys.* 83, 1057 (2011).
- [5] Y. Ando, Topological insulator materials, *Journal of the Physical Society of Japan* 82, 102001 (2013).
- [6] B. A. Bernevig, T. L. Hughes, and S.-C. Zhang, Quantum Spin Hall Effect and Topological Phase Transition in HgTe Quantum Wells, *Science* 314, 1757 (2006).
- [7] M. König, S. Wiedmann, C. Brüne, A. Roth, H. Buhmann, L. W. Molenkamp, X.-L. Qi, and S.-C. Zhang, Quantum Spin Hall Insulator State in HgTe Quantum Wells, *Science* 318, 766 (2007).
- [8] D. Hsieh, D. Qian, L. Wray, Y. Xia, Y. S. Hor, R. J. Cava, and M. Z. Hasan, A topological Dirac insulator in a quantum spin Hall phase, *Nature* 452, 970 (2008).
- [9] D. Hsieh, Y. Xia, D. Qian, L. Wray, J. H. Dil, F. Meier, J. Osterwalder, L. Patthey, J. G. Checkelsky, N. P. Ong, A. V. Fedorov, H. Lin, A. Bansil, D. Grauer, Y. S. Hor, R. J. Cava and M. Z. Hasan, A tunable topological insulator in the spin helical Dirac transport regime, *Nature* 460, 1101 (2009).
- [10] M. Z. Hasan and J. E. Moore, Three-Dimensional Topological Insulators, *Annual Review of Condensed Matter Physics* 2, 55 (2011).
- [11] L. Fu and C. L. Kane, Topological insulators with inversion symmetry, *Phys. Rev. B* 76, 045302 (2007).
- [12] L. Fu, C. L. Kane, and E. J. Mele, Topological Insulators in Three Dimensions, *Phys. Rev. Lett.* 98, 106803 (2007).
- [13] X. Wan, A. M. Turner, A. Vishwanath, and S. Y. Savrasov, Topological semimetal and Fermi-arc surface states in the electronic structure of pyrochlore iridates, *Phys. Rev. B* 83, 205101 (2011).
- [14] B. Q. Lv, H. M. Weng, B. B. Fu, X. P. Wang, H. Miao, J. Ma, P. Richard, X. C. Huang, L. X. Zhao, G. F. Chen, Z. Fang, X. Dai, T. Qian, and H. Ding, Experimental Discovery of Weyl Semimetal TaAs, *Phys. Rev. X* 5, 031013 (2015).
- [15] S.-Y. Xu, N. Alidoust, I. Belopolski, Z. Yuan, G. Bian, T.-R. Chang, H. Zheng, V. N. Strocov, D. S. Sanchez, G. Chang, C. L. Zhang, D. X. Mou, Y. Wu, L. Huang, C.-C. Lee, S.-M. Huang, B. K. Wang, A. Bansil, H.-T. Jeng, T. Neupert, A. Kaminski, H. Lin, S. Jia and M. Z. Hasan, Discovery of a Weyl fermion state with Fermi arcs in niobium arsenide, *Nature Physics* 11, 748 (2015).
- [16] Z. K. Liu, B. Zhou, Y. Zhang, Z. J. Wang, H. M. Weng, D. Prabhakaran, S.-K. Mo, Z. X. Shen, Z. Fang, X. Dai, Z. Hussainand, and Y. L. Chen, Discovery of a Three-Dimensional Topological Dirac Semimetal, *Nature Science* 343, 864 (2014).
- [17] L. Fu, Topological Crystalline Insulators, *Phys. Rev. Lett.* 106, 106802 (2011).
- [18] J.-P. Xu, C. Liu, M.-X. Wang, J. Ge, Z.-L. Liu, X. Yang, Y. Chen, Y. Liu, Z.-A. Xu, C.-L. Gao, D. Qian, F.-C. Zhang, and J.-F. Jia, Artificial Topological Superconductor by the Proximity Effect, *Phys. Rev. Lett.* 112, 217001 (2014).
- [19] P. Dziawa, B. J. Kowalski, K. Dybko, R. Buczko, A. Szczerbakow, M. Szot, E. Lusakowska, T. Balasubramanian, B. M. Wojek, M. H. Berntsen, O. Tjernberg and T. Story, Topological crystalline insulator states in  $Pb_{1-x}Sn_xSe$ , *Nature Materials* 11, 1023 (2012).
- [20] T. H. Hsieh, H. Lin, J. Liu, W. Duan, A. Bansil, and L. Fu, Topological crystalline insulators in the SnTe material class, *Nature Communications* 3, 982 (2012).
- [21] Y. Tanaka, Z. Ren, T. Sato, K. Nakayama, S. Souma, T. Takahashi, K. Segawa, and Y. Ando, Experimental realization of a topological crystalline insulator in SnTe, *Nature Physics* 8, 800 (2012).
- [22] M. V. Berry, Quantal phase factors accompanying adiabatic changes, *Proceedings of the Royal Society of London. A. Mathematical and Physical Sciences* 392, 45 (1984).
- [23] M.Kohmoto, Topological invariant and the quantization of the Hall conductance, *Annals of Physics* 160, 343 (1985)
- [24] D. Xiao, M.-C. Chang, and Q. Niu, Berry phase effects on electronic properties, *Rev. Mod. Phys.* 82, 1959 (2010).
- [25] J. Zak, Berry's phase for energy bands in solids, *Phys. Rev. Lett.* 62, 2747 (1989).
- [26] L. Lu, J. D. Joannopoulos, and M. Soljacic, Topological photonics, *Nature Photonics* 108, 821 (2014).
- [27] T. Ozawa, H. M. Price, A. Amo, N. Goldman, M. Hafezi, L. Lu, M. C. Rechtsman, D. Schuster, J. Simon, O. Zilberberg, and I. Carusotto, Topological photonics, *Rev. Mod. Phys.* 91, 015006 (2019).
- [28] A. B. Khanikaev, S. Hossein Mousavi, W.-K. Tse, M. Kargarian, A. H. MacDonald, and G. Shvets, Photonic topological insulators, *Nature Materials* 12, 233 (2013).
- [29] A. B. Khanikaev and G. Shvets, Two-dimensional topo-

- logical photonics, *Nature Photonics* 11, 763 (2017).
- [30] X.-C. Sun, C. He, X.-P. Liu, M.-H. Lu, S.-N. Zhu, and Y.-F. Chen, Two-dimensional topological photonic systems, *Progress in Quantum Electronics* 55, 52 (2017).
- [31] T. Ozawa, H. M. Price, N. Goldman, O. Zilberberg, and I. Carusotto, Synthetic dimensions in integrated photonics: From optical isolation to four-dimensional quantum Hall physics, *Phys. Rev. A* 93, 043827 (2016).
- [32] L.-H. Wu and X. Hu, Scheme for Achieving a Topological Photonic Crystal by Using Dielectric Material, *Phys. Rev. Lett.* 114, 223901 (2015).
- [33] S. Raghu and F. D. M. Haldane, Analogs of quantum-Hall-effect edge states in photonic crystals, *Phys. Rev. A* 78, 033834 (2008).
- [34] S. A. Dyakov, A. Baldycheva, T. S. Perova, G. V. Li, E. V. Astrova, N. A. Gippius, and S. G. Tikhodeev, Surface states in the optical spectra of two-dimensional photonic crystals with various surface terminations, *Phys. Rev. B* 86, 115126 (2012).
- [35] F. D. M. Haldane and S. Raghu, Possible Realization of Directional Optical Waveguides in Photonic Crystals with Broken Time-Reversal Symmetry, *Phys. Rev. Lett.* 100, 013904 (2008).
- [36] T. Ma, A. B. Khanikaev, S. H. Mousavi, and G. Shvets, Guiding Electromagnetic Waves around Sharp Corners: Topologically Protected Photonic Transport in Metawaveguides, *Phys. Rev. Lett.* 114, 127401 (2015).
- [37] M. C. Rechtsman, J. M. Zeuner, Y. Plotnik, Y. Lumer, D. Podolsky, F. Dreisow, S. Nolte, M. Segev, and A. Szameit, Photonic Floquet topological insulators, *Nature* 496, 196 (2013).
- [38] M. Verbin, O. Zilberberg, Y. E. Kraus, Y. Lahini, and Y. Silberberg, Observation of Topological Phase Transitions in Photonic Quasicrystals, *Phys. Rev. Lett.* 110, 076403 (2013).
- [39] H. Zhong, Y. V. Kartashov, A. Szameit, Y. Li, C. Liu, and Y. Zhang, Theory of topological corner state laser in Kagome waveguide arrays, *APL Photonics* 6, 040802 (2021).
- [40] L. Yuan, Q. Lin, M. Xiao, and S. Fan, Synthetic dimension in photonics, *Optica* 5, 1396 (2018).
- [41] M. Hafezi, E. A. Demler, M. D. Lukin, and J. M. Taylor, Robust optical delay lines with topological protection, *Nature Physics* 7, 907 (2011).
- [42] M. Hafezi, S. Mittal, J. Fan, A. Migdall, and J. M. Taylor, Imaging topological edge states in silicon photonics, *Nature Photonics* 7, 1001 (2013).
- [43] S. Peng, N. J. Schilder, X. Ni, J. van de Groep, M. L. Brongersma, A. Alu, A. B. Khanikaev, H. A. Atwater, and A. Polman, Probing the Band Structure of Topological Silicon Photonic Lattices in the Visible Spectrum, *Phys. Rev. Lett.* 122, 117401 (2019).
- [44] D. Leykam and D. G. Angelakis, Photonic band structure design using persistent homology, *APL Photonics* 6, 030802 (2021).
- [45] J. Noh, S. Huang, K. P. Chen, and M. C. Rechtsman, Observation of Photonic Topological Valley Hall Edge States, *Phys. Rev. Lett.* 120, 063902 (2018).
- [46] D. Smirnova, D. Leykam, Y. Chong, and Y. Kivshar, Nonlinear topological photonics, *Applied Physics Reviews* 7, 021306 (2020).
- [47] R. Secondo, A. Ball, B. Diroll, D. Fomra, K. Ding, V. Avrutin, U. Ozgr, D. O. Demchenko, J. B. Khurgin, and N. Kinsey, Deterministic modeling of hybrid nonlinear effects in epsilon-near-zero thin films, *Applied Physics Letters* 120, 031103 (2022).
- [48] N. Chang, S. Gundogdu, D. Leykam, D. G. Angelakis, S. Kou, S. Flach, and A. Maluckov, Nonlinear Bloch wave dynamics in photonic Aharonov-Bohm cages, *APL Photonics* 6, 030801 (2021).
- [49] W. Zhang, X. Chen, Y. V. Kartashov, V. V. Konotop, and F. Ye, Coupling of Edge States and Topological Bragg Solitons, *Phys. Rev. Lett.* 123, 254103 (2019).
- [50] C.-E. Bardyn, T. Karzig, G. Refael, and T. C. H. Liew, Topological polaritons and excitons in garden-variety systems, *Phys. Rev. B* 91, 161413 (2015).
- [51] Y. Hadad, A. B. Khanikaev, and A. Alú, Self-induced topological transitions and edge states supported by nonlinear staggered potentials, *Phys. Rev. B* 93, 155112 (2016).
- [52] D. N. Christodoulides and R. I. Joseph, Array waveguide devices; Coupled mode theory; Modulational instabilities; Refractive index; Self focusing; Self phase modulation, *Opt. Lett.* 13, 794 (1988).
- [53] L. Fan, J. Wang, L. T. Varghese, H. Shen, B. Niu, Y. Xuan, A. M. Weiner, and M. Qi, An All-Silicon Passive Optical Diode, *Science* 335, 447 (2012).
- [54] Y. Yu, Y. Chen, H. Hu, W. Xue, K. Yvind, and J. Mork, Nonreciprocal transmission in a nonlinear photonic-crystal Fano structure with broken symmetry, *Laser & Photonics Reviews* 9, 241 (2015).
- [55] F. Zangeneh-Nejad and R. Fleury, Nonlinear Second-Order Topological Insulators, *Phys. Rev. Lett.* 123, 053902 (2019).
- [56] R. Chaunsali, H. Xu, J. Yang, P. G. Kevrekidis, and G. Theocharis, Stability of topological edge states under strong nonlinear effects, *Phys. Rev. B* 103, 024106 (2021).
- [57] R. W. Bomantara,  $Z_4$  parafermion  $\pm\pi/2$  modes in an interacting periodically driven superconducting chain, *Phys. Rev. B* 104, L121410 (2021).
- [58] D. A. Smirnova, L. A. Smirnov, E. O. Smolina, D. G. Angelakis, and D. Leykam, Gradient catastrophe of nonlinear photonic valley-Hall edge pulses, *Phys. Rev. Research* 3, 043027 (2021).
- [59] Q. Tang, B. Ren, V. O. Kompanets, Y. V. Kartashov, Y. Li, and Y. Zhang, Array waveguide devices; Bright solitons; Domain wall solitons; Modulational instabilities; Nonlinear effects; Solitons, *Opt. Express* 29, 39755 (2021).
- [60] D. A. Smirnova, L. A. Smirnov, D. Leykam, and Y. S. Kivshar, Topological Edge States and Gap Solitons in the Nonlinear Dirac Model, *Laser & Photonics Reviews* 13, 1900223 (2019).
- [61] B. Wu and Q. Niu, Nonlinear Landau-Zener tunneling, *Phys. Rev. A* 61, 023402 (2000).
- [62] J. Liu, L. Fu, B.-Y. Ou, S.-G. Chen, D.-I. Choi, B. Wu, and Q. Niu, Theory of nonlinear Landau-Zener tunneling, *Phys. Rev. A* 66, 023404 (2002).
- [63] B. Wu, R. B. Diener, and Q. Niu, Bloch waves and Bloch bands of Bose-Einstein condensates in optical lattices, *Phys. Rev. A* 65, 025601 (2002).
- [64] W.-M. Liu, B. Wu, and Q. Niu, Nonlinear Effects in Interference of Bose-Einstein Condensates, *Phys. Rev. Lett.* 84, 2294 (2000).
- [65] M. Machholm, C. J. Pethick, and H. Smith, Band structure, elementary excitations, and stability of a Bose-Einstein condensate in a periodic potential, *Phys. Rev. A* 67, 053613 (2003).

- [66] J. Liu, B. Wu, and Q. Niu, Nonlinear Evolution of Quantum States in the Adiabatic Regime, *Phys. Rev. Lett.* 90, 170404 (2003).
- [67] B. Liu, L.-B. Fu, S.-P. Yang, and J. Liu, Josephson oscillation and transition to self-trapping for Bose-Einstein condensates in a triple-well trap, *Phys. Rev. A* 75, 033601 (2007).
- [68] X. X. Yi, X. L. Huang, and W. Wang, Loschmidt echo and Berry phase around degeneracies in nonlinear systems, *Phys. Rev. A* 77, 052115 (2008).
- [69] Y. Zhang, Z. Gui, and Y. Chen, Nonlinear dynamics of a spin-orbit-coupled Bose-Einstein condensate, *Phys. Rev. A* 99, 023616 (2019).
- [70] T. Tuloup, R. W. Bomantara, C. H. Lee, and J. Gong, Nonlinearity induced topological physics in momentum space and real space, *Phys. Rev. B* 102, 115411 (2020).
- [71] Y. Zhang, Z. Chen, B. Wu, T. Busch, and V. V. Konotop, Asymmetric Loop Spectra and Unbroken Phase Protection due to Nonlinearities in  $\mathcal{PT}$ -Symmetric Periodic Potentials, *Phys. Rev. Lett.* 127, 034101 (2021).
- [72] S. B. Koller, E. A. Goldschmidt, R. C. Brown, R. Wyllie, R. M. Wilson, and J. V. Porto, Nonlinear looped band structure of Bose-Einstein condensates in an optical lattice, *Phys. Rev. A* 94, 063634 (2016).
- [73] Q. Guan, M. K. H. Ome, T. M. Bersano, S. Mossman, P. Engels, and D. Blume, Nonexponential Tunneling due to Mean-Field-Induced Swallowtails, *Phys. Rev. Lett.* 125, 213401 (2020).
- [74] J. R. Tempelman, K. H. Matlack, and A. F. Vakakis, Topological protection in a strongly nonlinear interface lattice, *Phys. Rev. B* 104, 174306 (2021).
- [75] Y. Hadad, J. C. Soric, A. B. Khanikaev, and A. Alú, Self-induced topological protection in nonlinear circuit arrays, *Nature Electronics* 1, 178 (2018).
- [76] D. Zhou, D. Z. Rocklin, M. Leamy, and Y. Yao, Topological invariant and anomalous edge modes of strongly nonlinear systems, *Nature Communications* 13, 3379 (2022).
- [77] R. Chaunsali, H. Xu, J. Yang, P. G. Kevrekidis, and G. Theoharis, Stability of topological edge states under strong nonlinear effects, *Phys. Rev. B* 103, 024106 (2021).
- [78] L. Jezequel and P. Delplace, Nonlinear edge modes from topological one-dimensional lattices, *Phys. Rev. B* 105, 035410 (2022).
- [79] B. Many Manda, R. Chaunsali, G. Theoharis, and C. Skokos, Nonlinear topological edge states: From dynamic delocalization to thermalization, *Phys. Rev. B* 105, 104308 (2022).
- [80] Z. Chen and B. Wu, Bose-Einstein Condensate in a Honeycomb Optical Lattice: Fingerprint of Superfluidity at the Dirac Point, *Phys. Rev. Lett.* 107, 065301 (2011).
- [81] R. W. Bomantara, W. Zhao, L. Zhou, and J. Gong, Nonlinear Dirac cones, *Phys. Rev. B* 96, 121406 (2017).
- [82] D. Leykam, E. Smolina, A. Maluckov, S. Flach, and D. A. Smirnova, Probing Band Topology Using Modulational Instability, *Phys. Rev. Lett.* 126, 073901 (2021).
- [83] F. Li, K. Xue, and X. Yi, Nonlinear Topological Effects in Optical Coupled Hexagonal Lattice, *Entropy* 23 (2021).
- [84] P. He and Z. Li, Nonlinear Bloch-Zener oscillations for Bose-Einstein condensates in a Lieb optical lattice, *New Journal of Physics* 22, 063031 (2020).
- [85] S. Deng, Y. Chu, and Q. Zhu, Moiré exciton condensate: nonlinear Dirac point, broken-symmetry Bloch waves and unusual optical selection rules, arXiv:2207.02415 (2022).
- [86] B. A. Bernevig, *Topological Insulators and Topological Superconductors* (Princeton University Press, Princeton, 2013).
- [87] S.-Q. Shen, *Topological Insulators: Dirac Equation in Condensed Matters* (Springer Berlin, Heidelberg, 2012).